

Accepted for publication in the June 2010 Astronomical Journal

Ultracool Field Brown Dwarf Candidates Selected at $4.5\mu\text{m}$

Peter R. M. Eisenhardt¹, Roger L. Griffith¹, Daniel Stern¹, Edward L. Wright²,
Matthew L. N. Ashby³, Mark Brodwin^{3,4}, Michael J. I. Brown⁵, R. S. Bussmann⁶, Arjun Dey⁷,
A. M. Ghez², Eilat Glikman⁸, Anthony H. Gonzalez⁹, J. Davy Kirkpatrick¹⁰, Quinn Konopacky²,
Amy Mainzer¹, David Vollbach⁹, Shelley A. Wright¹¹

ABSTRACT

We have identified a sample of cool field brown dwarf candidates using IRAC data from the *Spitzer* Deep, Wide-Field Survey (SDWFS). The candidates were selected from 400,000 SDWFS sources with $[4.5] \leq 18.5$ mag and required to have $[3.6] - [4.5] \geq 1.5$ and $[4.5] - [8.0] \leq 2.0$ on the Vega system. The first color requirement selects objects redder than all but a handful of presently known brown dwarfs with spectral classes later than T7, while the second eliminates 14 probable reddened AGN. Optical detection of 4 of the remaining 18 sources implies they are likely also AGN, leaving 14 brown dwarf candidates. For two of the brightest candidates (SDWFS J143524.44+335334.6 and SDWFS J143222.82+323746.5), the spectral energy distributions including near-infrared detections suggest a spectral class of \sim T8. The proper motion is $< 0''.25 \text{ yr}^{-1}$, consistent with expectations for a luminosity inferred distance of > 70 pc. The reddest brown dwarf candidate (SDWFS J143356.62+351849.2) has $[3.6] - [4.5] = 2.24$ and $H - [4.5] > 5.7$, redder than any published brown dwarf in these colors, and may be the first example of the elusive Y-dwarf spectral class. Models from Burrows et al. (2003)

¹Jet Propulsion Laboratory, California Institute of Technology, MS 169-327, 4800 Oak Grove Drive, Pasadena, CA 91109 [e-mail: Peter.Eisenhardt@jpl.nasa.gov]

²University of California, Los Angeles, CA 90095

³Harvard-Smithsonian Center for Astrophysics, 60 Garden Street, Cambridge, MA 02138

⁴W. M. Keck Postdoctoral Fellow at the Harvard-Smithsonian Center for Astrophysics

⁵School of Physics, Monash University, Clayton, Victoria 3800, Australia

⁶Steward Observatory, University of Arizona, Tucson AZ 85721

⁷National Optical Astronomy Observatory, Tucson, AZ 85726

⁸Division of Physics, Math and Astronomy, California Institute of Technology, Pasadena, CA 91125

⁹Department of Astronomy, University of Florida, Gainesville, FL 32611

¹⁰Infrared Processing and Analysis Center, California Institute of Technology, Pasadena, CA 91125

¹¹Astronomy Department, University of California, Berkeley, CA 94709

predict larger numbers of cool brown dwarfs should be found for a Chabrier (2003) mass function. Suppressing the model [4.5] flux by a factor of two, as indicated by previous work, brings the Burrows models and observations into reasonable agreement. The recently launched Wide-field Infrared Survey Explorer (*WISE*) will probe a volume $\sim 40\times$ larger and should find hundreds of brown dwarfs cooler than T7.

Subject headings: surveys: infrared — stars: brown dwarfs — stars: individual (SD-WFS J142831.46+354923.1, SDWFS J143524.44+335334.6, SDWFS J143356.62+351849.2)

1. Introduction

Although first predicted to exist in 1963 (Kumar 1963; Hayashi & Nakano 1963), brown dwarfs were not discovered until decades later. The first viable brown dwarf candidate was GD 165B (Becklin & Zuckerman 1988), an L dwarf whose exact nature as hydrogen-burning star or brown dwarf has yet to be ascertained (Kirkpatrick et al. 1999). The first undisputed brown dwarf, and the first T dwarf, was Gl 229B (Nakajima et al. 1995), whose telltale methane absorption implied an effective temperature too low for a normal star. In the late 1990’s the advent of large-area surveys with near-infrared capability – the Two Micron All-Sky Survey (2MASS; Skrutskie et al. 2006), the Sloan Digital Sky Survey (SDSS; York et al. 2000), and the Deep Near-Infrared Survey of the Southern Sky (DENIS; Epchtein et al. 1997) – uncovered hundreds more examples and enabled the study of brown dwarfs as a population in their own right (Kirkpatrick 2005)¹.

The latest spectral type brown dwarfs currently known are T8 and T9 dwarfs found by 2MASS, the United Kingdom Infrared Deep Sky Survey (UKIDSS; Lawrence et al. 2007), and the Canada France Brown Dwarf Survey (Delorme et al. 2008a). The coolest of these have effective temperatures of ~ 550 K and implied masses of around 15-35 M_{Jupiter} for assumed ages of 1-5 Gyr (Warren et al. 2007; Burgasser et al. 2008; Burningham et al. 2008; Delorme et al. 2008b; Leggett et al. 2009). Cooler field brown dwarfs must exist, however, as objects of much lower implied mass have been identified in young clusters such as the Orion Nebula Cluster (Zapatero Osorio et al. 2002; Weights et al. 2008), Upper Scorpius (Lodieu et al. 2007) and Chamaeleon I (Luhman et al. 2005), or as companions to other low-mass cluster members (e.g., Luhman et al. 2006)². Finding and characterizing such colder field objects will set important boundary conditions on star formation processes and determine the total amount of mass in stars, a key ingredient in modeling galaxy formation. Identifying examples of such objects is also important to the study of very cold, planet-like atmospheres. A leading question is whether a new spectral class beyond T, dubbed “Y”, will be needed (Kirkpatrick 2008).

¹see DwarfArchives.org for a full list

²see also <http://vlbinaries.org>

The two shortest wavelength bands in the *Spitzer* Infrared Array Camera (IRAC; Fazio et al. 2004) were designed to identify cool brown dwarfs from the signature due to strong methane absorption at $3.6\mu\text{m}$ coupled with a relative lack of absorption at $4.5\mu\text{m}$ (Fazio et al. 1998). Finding the coolest and nearest brown dwarfs is a key objective for the *Wide-field Infrared Survey Explorer* (WISE, Liu et al. 2008), which launched 2009 Dec. 14, and hence two of its four imaging bands are at similar wavelengths (3.4 and $4.6\mu\text{m}$). While a number of brown dwarf companions have been found using IRAC, prior to the *Spitzer* Deep, Wide-Field Survey (SDWFS; Ashby et al. 2009) only a single isolated field brown dwarf, of spectral class T4.5, has been identified to date on the basis of IRAC data (Stern et al. 2007). This object, IRAC J1429050.8+333011, was found in the IRAC Shallow Survey (Eisenhardt et al. 2004) and was required to be unresolved in complementary NOAO Deep Wide-Field Survey (NDWFS; Jannuzi & Dey 1999) *I*-band data, which necessitated $I < 23$. Here we remove the limitation of requiring optical detection and use the deeper and more reliable SDWFS IRAC data to search for cooler brown dwarf candidates.

2. Data and Selection Criteria

2.1. SDWFS

SDWFS is a four epoch Legacy survey of 10 square degrees in Boötes using the IRAC instrument. Each epoch covers the entire field with three exposures separated by hours, each 30s long, providing 12 observations at each sky location in all four IRAC bands. The first epoch is the IRAC Shallow Survey (Eisenhardt et al. 2004) from January 2004, and the last was obtained in March 2008. The publicly released³, full-depth (i.e., four epoch) catalogs contain 8.2, 6.7, 3.1, and 1.8×10^5 distinct sources detected at 3.6, 4.5, 5.8, and $8.0 \mu\text{m}$, of which 6.70, 5.28, 1.34, and 0.92×10^5 exceed the average 5σ , aperture-corrected limits of 20.0, 19.0, 16.7, and 15.9 Vega mag. The uncertainties properly account for errors due to correlated pixels that arise during coadding. See Ashby et al. (2009) for details of the SDWFS observations and analysis. We use the notation [3.6], [4.5], [5.8], and [8] for the Vega magnitudes in the four IRAC bands.

Since the Boötes field is at Galactic latitude 67 degrees, the bulk of the [3.6] and [4.5] sources at these fluxes are extragalactic. Figure 13 of Ashby et al. (2009) shows nearly all of the sources have $-0.1 < [3.6] - [4.5] < 1$, a range which includes the expected colors of galaxies out $z > 3$. AGN can extend to somewhat redder [3.6] – [4.5] colors, while occupying a narrow range in [5.8] – [8.0] (Fig. 1 of Stern et al. 2005).

Cool brown dwarf candidates were identified from the 671,688 SDWFS $4.5\mu\text{m}$ sources using the following selection criteria: (i) $[4.5] \leq 18.5$ (419,980 sources remaining), (ii) $[3.6] - [4.5] \geq 1.5$ (2,364 sources remaining), (iii) coverage of $\geq 10 \times 30$ s in a $4''.2 \times 4''.2$ (5×5 resampled pixels)

³<http://ssc.spitzer.caltech.edu/spitzermission/observingprograms/legacy/sdwfs>

region around each source in both the 3.6 and 4.5 μm bands (52 sources remaining). Photometry was measured in 3'' diameter apertures, corrected to 12'' radius total Vega magnitudes. The [4.5] magnitude limit provides $\sim 65\%$ completeness (Ashby et al. 2009), and ~ 0.3 mag color accuracy for objects which satisfy the color limits. The second criterion was selected to avoid confusion with AGN, which are rare at $[3.6] - [4.5] > 1.5$ (Stern et al. 2005), and should identify brown dwarfs later than approximately spectral type T7 (Patten et al. 2006). The coverage map requirement reduces spurious sources selected near the edges of the survey field, or heavily affected by cosmic rays.

The 52 candidates identified with these three criteria were visually inspected using separate images and photometry available for each of the four SDWFS epochs, and 20 were classified as artifacts due to glints, cosmic rays, diffraction spikes, or muxbleed trails from bright stars. Although all of the 52 candidates were observed in epoch one (the IRAC Shallow Survey), with only three exposures there are many more spurious candidates at these extreme colors, making it impractical and ambiguous to visually screen them. The T4.5 brown dwarf found by Stern et al. (2007) used independent optical NDWFS data to ensure reliability, but for cooler brown dwarfs, optical detection is not expected. The additional SDWFS exposures enable reliable detection using IRAC data alone.

Many of the remaining 32 sources were suspiciously prominent at 5.8 μm and 8 μm , leading to the imposition of an additional criterion: (iv) $[4.5] - [8.0] \leq 2.0$. This final criterion is designed to exclude heavily reddened AGN or dust obscured galaxies (DOGs; Dey et al. 2008) as well as AGB stars which meet the second criterion, but continue to brighten in the longer wavelength IRAC passbands, unlike brown dwarfs (Figure 1). Left-pointing arrows in Figure 1 are based on two sigma upper limits at [8.0] based on the SDWFS depths in Ashby et al. (2009).

This selection leaves the 18 candidates shown in Table 1. Two are noted as less robust based on visual inspection, and four show evidence of being DOG variants (§2.2), and hence are grouped separately at the bottom of Table 1. SDWFS images are available via the link in the footnote provided earlier in this section. Figure 2 shows the brightest and reddest candidates, as well as the reddest DOG (SDWFS J143819.58+340957.3, the only DOG with $[3.6] - [4.5] > 2$).

2.2. Data at Other Wavelengths

Most of the candidates have NDWFS photometry available in B_W , R , and I , from the NDWFS, and JHK_s photometry from the NEWFIRM survey of the field with the KPNO 4m (Gonzalez et al., in prep.), as shown in Table 1. The depth of these groundbased data are not as uniform as the SDWFS IRAC data, and hence optical and near-IR limits were estimated for each undetected source. When the estimated error exceeded 0.5 mag, two sigma upper limits above the measured flux (or 0 if measured flux was negative) were calculated from the errors in 3'' diameter apertures, corrected to total magnitudes, for the appropriate location in the NDWFS and NEWFIRM data.

Four of the candidates have faint or marginal detections in B_W (one in R as well), and some of those have hints of detections in IRAC 5.8 or $8.0\mu\text{m}$. Optical detections giving $B_W - [4.5] \sim 7$ to 8 are not expected even for warm brown dwarfs, so it is likely these are variants of DOGs, which tend to be $z \sim 2$ galaxies and are detectable in B_W from their Ly- α emission. Indeed, of the 14 objects classified as DOGs because they passed the first three selection criteria and the visual inspection, but failed the fourth, 10 are detected in B_W . Hence we have separated the four objects with faint optical detections in Table 1 from the other SDWFS brown dwarf candidates with the heading “Likely AGN.”

All but one of the 18 objects in Table 1 has *Spitzer* MIPS $24\mu\text{m}$ photometry available (Houck et al. 2005), and none were detected to a level of 0.3 mJy. In contrast, of the 13 DOG candidates observed at $24\mu\text{m}$, 10 were detected.

Likewise, none of the brown dwarf candidates were detected by the *Chandra X-Ray Observatory* survey of the Boötes field (XBoötes; Kenter et al. 2005) or at radio wavelengths by either the Faint Images of the Radio Sky at Twenty centimeters survey (FIRST; Becker et al. 1995) or by the deeper Westerbork 1.4 GHz observations of 7 deg^2 of Boötes reported in de Vries et al. (2002). Four DOG candidates were detected at radio wavelengths, one of which was also detected by XBoötes. That MIPS-selected source, SDWFS J143644.23+350627.0, has a redshift of $z = 1.95$ from *Spitzer* Infrared Spectrograph observations (Houck et al. 2005).

2.3. Near-IR Follow-Up

The brightest two candidates (see Figure 2) were targeted for additional follow-up using the Wide-field Infrared Camera (WIRC; Wilson et al. 2003) at the Palomar 5.08 m telescope on UT 2008 Aug 25 (SDWFS J143524.44+335334.6, hereafter SDWFS1435+33) and UT 2008 Aug 28 (SDWFS J142831.46+354923.1, hereafter SDWFS1428+35). Dithered sets of $4 \times 30\text{s}$ images were taken with exposure times (seeing) of 36m ($1''.1$) at J and 54m ($1''.0 - 1''.2$) at H for SDWFS1428+35, and 54m ($1''.3$) at H for SDWFS1435+33. Photometry was calibrated using ~ 10 2MASS sources in each field. No significant detections were obtained. Using the rms variation in $3''$ diameter apertures, the 2σ aperture corrected limits are $J > 21.9$ and $H > 21.4$ for SDWFS1428+35. For SDWFS1435+33 the Palomar data yield $H > 21.3$, but the NEWFIRM survey provides detections at $J = 21.16 \pm 0.13$ and $H = 21.09 \pm 0.48$ as listed in Table 1. The NEWFIRM survey also detected SDWFS J143222.82+323746.5 at $J = 21.17 \pm 0.18$. Both the SDWFS1435+33 and SDWFS1432+32 detections are at levels expected for ultracool brown dwarfs, and all of the objects in Table 1 have near-IR to $[4.5]$ colors or limits consistent with late T dwarfs (§3.2).

The reddest candidate identified (SDWFS J143356.62+351849.2, hereafter SDWFS1433+35) was targeted for followup with the NIRC2 camera (P.I. K. Matthews) on the Keck II telescope using laser guide star adaptive optics (Wizinowich et al. 2006; van Dam et al. 2006) on UT 2009 June 11. A total of 42 minutes of integration using 3 minute exposures and a pixel scale of $0''.0397$ in H

was obtained under photometric conditions and $0''.5$ seeing. An $R = 17.6$ star $20''.7$ to the West was used to provide tip-tilt correction. The point source FWHM in the combined image is $0''.12$, and the estimated Strehl ratio is 0.2 at the location of SDWFS1433+35. The field of view was positioned so that the tip-tilt star was in the field to provide a photometric and astrometric reference, but it was slightly saturated in 3 minutes, so additional 4×30 s coadded exposures were obtained to calibrate the photometry. No detection of SDWFS1433+35 is apparent in the combined image (Figure 3). We estimate $H > 24.2$ for SDWFS1433+35, by comparing to scaled down versions of the photometric tip-tilt star (which has $H = 16.19$ from 2MASS) added into the combined image.

Figure 4 shows the SEDs for SDWFS1435+33 and SDWFS1433+35.

2.4. Proper Motions

With low intrinsic luminosity, cool brown dwarfs should be nearby and thus may have detectable proper motions in the four years spanned by SDWFS. Sources with large proper motion might even be rejected from the SDWFS catalog because they move between epochs. To allow for this, a search was made for objects in each of the four SDWFS epochs which satisfied criteria (i) and (ii), and whose positions matched to within $10''$. This search did not find any sources not already identified using the full SDWFS dataset as described above.

The average astrometric frame offset between SDWFS epochs is $\approx 0''.17$, with a standard deviation of $\approx 0''.35$ for sources with $[4.5] < 18$ (Ashby et al. 2009). For sources near the $[4.5] = 18.5$ limit of the present sample, a standard deviation of $\approx 0''.55$ is appropriate. None of the brown dwarf candidates in Table 1 show significant ($\geq 3\sigma$) proper motions, implying proper motions $\mu \leq 0''.25 \text{ yr}^{-1}$ ($0''.4 \text{ yr}^{-1}$ for sources near the $[4.5] = 18.5$ limit).

Ashby et al. (2009) do find four SDWFS sources with proper motions of $\approx 0''.3 \text{ yr}^{-1}$, including two⁴ with $[3.6] - [4.5]$ colors appropriate for mid- to late-T brown dwarfs (Patten et al. 2006), but not meeting the $[3.6] - [4.5] \geq 1.5$ criterion. The NEWFIRM survey of the SDWFS field provides $J = 19.48$ and $H = 19.94$ in aperture corrected $4''$ diameter apertures for SDWFS J142723+330403, consistent with expectations for a T7 dwarf with $[4.5] = 16.96$.

3. Discussion

The SDWFS search confirms the impression from the IRAC Shallow Survey (Eisenhardt et al. 2004, Fig. 4b) that at high Galactic latitude, objects with IRAC colors as red as the coolest known

⁴SDWFS J142723+330403 was mistakenly identified with a nearby but unrelated NDWFS source in Ashby et al. (2009), and the $B_W RI$ photometry shown for this object in Table 26 of that paper is incorrect. Instead, only the NDWFS upper limits apply.

brown dwarfs are rare. Of 367,176 SDWFS sources meeting criteria (i) and (iii) in §2.1, less than one in ten thousand is a real source meeting criterion (ii), i.e. $([3.6] - [4.5] \geq 1.5$, equivalent to $F_\nu(4.5)/F_\nu(3.6) > 2.5$). Only two real objects have $[3.6] - [4.5] > 2$ — presumably the realm inhabited by the elusive Y-dwarfs — making them an order of magnitude rarer still. Although we were careful *not* to require [3.6] detection, all brown dwarf candidates, and all but one DOG (SDWFS J143819.58+340957.3 — Figure 2) are in fact clearly detected in [3.6].

A blackbody with $[3.6] - [4.5] \geq 1.5$ would have $T_{\text{BB}} \lesssim 500\text{K}$, while a power-law spectrum would need $\alpha > 4$ where $F_\nu \propto \nu^{-\alpha}$. Such spectra might arise from cool brown dwarfs or warm dust, or from obscuration of hotter spectra by dust. For brevity, we often substitute C for $[3.6] - [4.5]$ in the remainder of the discussion.

3.1. Dusty Sources

Dust enshrouded carbon stars and AGB stars (e.g. Cutri et al. 1989), or class 0 or I protostars (e.g. Enoch et al. 2009) can have very red IRAC colors due to warm dust emission (Figure 1). However for the $T_{\text{BB}} \lesssim 500\text{K}$ needed to produce $[3.6] - [4.5] \geq 1.5$, the corresponding $[4.5] - [8]$ is > 2.3 , violating criterion (iv). Significant emission from cooler dust is typical for such sources, which is even less consistent with the longer wavelength photometry for the brown dwarf candidates. Hence it is possible that some of the sources classified as DOGs may in fact be stellar.

Nevertheless Figure 1 shows that the locus of likely AGB stars from Robitaille et al. (2007) lies near the brown dwarf selection region, with three out of 23 with $C \equiv [3.6] - [4.5] \geq 1.5$ falling inside it. AGB stars associated with our Galaxy are unlikely contaminants, both due to their faintness and to the high Galactic latitude of the field (67 degrees). The absolute [4.5] magnitude of a typical AGB star is ~ -10 (Cutri et al. 1989), putting AGBs with the characteristic [4.5] ~ 18 values found in Table 1 at a distance of order 3 Mpc. Mauron (2008) finds three AGB stars more than 100 kpc from the Sun, presumably from the disruption of tidally captured dwarf galaxies. If this space density is typical, there could be of order 10 AGB stars in the SDWFS volume at a distance near 3 Mpc. However, using the NASA Extragalactic Database, we find no galaxies brighter than 15th mag (optical, i.e $\sim 1000\times$ less luminous than the Milky Way at 3 Mpc) and with redshifts < 1000 km/s within 5 degrees (~ 300 kpc at 3 Mpc) of the field.

Note that AGB stars are often large amplitude variables. Rejkuba et al. (2003) and Davidge & Rigaut (2004) find that most AGB stars in NGC 5128 and M32 respectively are variable. Rejkuba et al. (2003) give an average K band amplitude of 0.77 mag and a period of 395 days, similar to values found by Glass et al. (1995) for Galactic AGB stars. The threshold for the Robitaille et al. (2007) sources is a factor of two (0.75 mag). The peak to peak variation in the [4.5] mags between the four SDWFS epochs (which span four years) exceeds the factor of two level for two of the sources in Table 1. For one of these, SDWFS J143712.48+334516.5, inspection of the data shows this is because its [4.5] brightness is spuriously high in one epoch due to a cosmic ray in

the aperture, which was rejected in the combined 4-epoch measurement. For the other source, SDWFS J143821.36+353523.3, although the peak to peak variation is 1.5 mag, the rms is 0.66 mag, which is only slightly more than a one sigma excess above the median variability at [4.5] for this magnitude (Kozłowski et al. 2010). Because there is little evidence for excess variability in the Table 1 sources, and no obvious source for intergalactic AGB stars, we consider such stars unlikely to be a significant contaminant for our brown dwarf candidate sample.

Dey et al. (2008) describe a sample of 2603 objects in the Boötes field selected to have $R - [24] \geq 14$, which they interpret as dust obscured galaxies (DOGs). Of the 2491 DOGs from Dey et al. (2008) with SDWFS IRAC photometry, 12 have $C \geq 1.5$, but all of these have $[4.5] - [8] > 2$ so they do not appear in Table 1. DOGs with $C \geq 1.5$ (either from the Dey et al. (2008) $R - [24]$ selection, or classified as DOGs here from due to $[4.5] - [8] > 2$) are plotted as open circles in Figure 1. No attempt is made to distinguish AGN with $C > 1.5$ from DOGs, since DOGs include AGN. Objects plotted as dots in Figure 1 satisfy the Stern et al. (2005) AGN criteria. Of these four have $C > 1.5$, and with $[4.5] - [8] \sim 3$ they fall in the midst of the DOG colors.

Dey et al. (2008) suggest the $24\mu\text{m}$ emission arises from warm dust heated by an AGN for the brighter sources, or from redshifted PAH emission at $z \sim 2$ for the fainter sources. The red IRAC colors for these fainter DOGs are likely due to obscuration of stellar light by dust. We estimate $A_V \gtrsim 6$ to produce $C \geq 1.5$ at $z \sim 2$. For the reddest DOG, SDWFS J143819.58+340957.3 (Figures 2 and 4), A_V well above 10 is indicated. As noted in §2.2, *none* of the objects in Table 1 are detected at $24\mu\text{m}$, while of the 14 sources classified here as DOGs from IRAC photometry (i.e $C \geq 1.5$ and $[4.5] - [8] > 2$), 10 of the 13 observed at $24\mu\text{m}$ were detected.

The 14 IRAC-classified DOGs were also detected in B_W in 9 cases, likely due to redshifted Ly- α emission, with 8 of the B_W detected objects having detections in R and I as well. The bottom portion of Table 1 lists three brown dwarf candidates (based on their IRAC photometry) with faint optical detections, and a fourth with a marginal optical detection, under the heading “Likely AGN.” These have been marked with shaded gray circles in Figure 1 to indicate that they are likely DOG variants. The potential for additional DOG/AGN contamination of the sample is discussed in §3.3.

3.2. Brown Dwarfs

Even for $T_{\text{eff}} < 500\text{K}$, brown dwarf spectra are expected to have $[4.5] - [8] < 2$ due to molecular absorption features (Figures 1 and 4, Burrows et al. 2003). If the sources in Table 1 are brown dwarfs, they have spectral classes later than T6, based on their $[3.6] - [4.5]$ colors (Figure 10, Patten et al. 2006). Only two of the 86 sources in Patten et al. (2006) have $C \equiv [3.6] - [4.5] \geq 1.5$: GJ 570D (T7.5) with a color of 1.68, and 2MASS 0415-0935 (T8.0) with a color of 1.82. At the time this paper was submitted, only three other brown dwarfs had colors this red: ULAS0034 with a color of 1.81 and spectral class T8.5 (Warren et al. 2007); ULAS1335 ($C = 2.05$, T9; Burningham

et al. 2008); and 2MASS 0939-24 ($C = 2.10$, a possible T8 binary; Burgasser et al. 2008)⁵. If it is confirmed, with $C = 2.24$ SDWFS1433+35 would have the reddest IRAC color of any brown dwarf yet found (Figure 1).

While the optical photometry does not reach the depths expected for T and late L dwarfs with $[4.5] \gtrsim 18$, the typical $I - [4.5] \gtrsim 6$ limits argue against the sources in Table 1 being significantly hotter than brown dwarfs. From Figure 8 of Hawley et al. (2002) and Fig. 10 of Patten et al. (2006), the onset of L dwarfs is at $i - [4.5] \sim 6.2$, equivalent to $I - [4.5] \sim 5.8$.

The $J - [4.5]$ color ranges from 2.49 to 3.99 for the previously published brown dwarfs with $C \geq 1.5$. For SDWFS1435+33 we find $J - [4.5] = 3.56$, which together with $C = 1.84$ is very similar to the observed values for ULAS0034. Detailed modeling of ULAS0034 lead Warren et al. (2007) and Leggett et al. (2009) to conclude that it has $T_{\text{eff}} \approx 600\text{K}$. For SDWFS1432+32 the $J - [4.5] = 3.11$ and $C = 1.91$ are each about 0.1 mag redder than the corresponding 2MA 0415-0935 (T8.0) values. Figure 4 shows the photometry for SDWFS1435+33 overplotted with a 600K model from Burrows et al. (2003). The $J - [4.5]$ limits for other brown dwarf candidates range from > 2.9 to > 4.4 , consistent with spectral classes beyond T6.

Burningham et al. (2008), Warren et al. (2007), and Leggett et al. (2010) suggest that $H - [4.5]$ is tightly correlated with T_{eff} . Figure 5 shows $H - [4.5]$ as a function of spectral type. The published brown dwarfs with $C \geq 1.5$ have $H - [4.5]$ colors ranging from 2.98 to 4.34, while the 2σ limits here range from > 2.1 to > 3.7 (> 5.7 for SDWFS1433+35 see below), consistent with spectral classes beyond T5. For SDWFS1435+33 $H - [4.5] = 3.49$ is similar to the T8 brown dwarf 2MA 0415-0935. We include SDWFS1432+32 in figure 5 as a grey-shaded point with $H - [4.5] = 3.46 \pm 0.7$. This assumes $J - H \sim -0.35$ based on photometry for late-T objects from Patten et al. (2006) and Leggett et al. (2010) together with our $J = 21.17$ detection to estimate $H = 21.52$, with the error bar consistent with the observed 2σ limit of $H > 20.8$.

The available K_s data offer fewer constraints than J and H . The published brown dwarfs with $C \geq 1.5$ have $K - [4.5]$ colors ranging from 2.98 to 5.17, while the 2σ limits here range from $K_s > 1.1$ to > 2.4 , consistent with spectral classes beyond L5.

From their $J - [4.5]$, $H - [4.5]$, and $[3.6] - [4.5]$ colors and limits, we associate a spectral class of T8 for SDWFS1435+33, and (more tentatively) T8.5 for SDWFS1432+32. Assuming $M_{4.5} = 13.5$ for SDWFS1435+33 (based on Patten et al. 2006), the luminosity distance is ~ 70 pc. As noted in §2.4, neither source shows significant proper motion, with an estimated $0''.25 \text{ yr}^{-1}$ limit for sources with $[4.5] < 18$. This is unsurprising, since typical proper motions should be $\sim 0''.1 \text{ yr}^{-1}$ at this distance, using an average tangential velocity from a volume-limited sample of stars of 37 km s^{-1} (Reid 1997, or $\sim 4 \text{ AU}$ in 6 months).

⁵After submission, five others appeared in Leggett et al. (2010): 2MA 0348-60, $C = 1.53$, T7; ULAS 2321+13, $C = 1.64$, T7.5; ULAS 1238+09, $C = 1.75$, T8.5; 2MA 1114-26, $C = 1.78$, T7.5; and Wolf 940B, $C = 2.01$, T8.5.

With $C = 2.24$, $[4.5] - [8] < 1.6$, and $H - [4.5] > 5.7$, the SED for SDWFS1433+35 falls in previously unpopulated regions of color space (Figures 1 and 5), and hence this object may be a member of the long-sought Y-dwarf class. Figure 4 shows a 400K Burrows et al. (2003) model which roughly agrees with the observations for SDWFS1433+35. If the 1.3 mag drop in [4.5] luminosity between the 400K and 600K Burrows et al. (2003) models is applicable, $M_{4.5} \sim 15$ for SDWFS1433+35 implying a distance ~ 50 pc. Again this is consistent with the $0''.4 \text{ yr}^{-1}$ proper motion limit noted in §2.4 for the $[4.5] = 18.47$ mag of SDWFS1433+35, vs. the typical expected proper motion of $\sim 0''.15 \text{ yr}^{-1}$ at 50 pc. Alternative explanations for SDWFS1433+35 must account for the non-detections in [5.8], [8], and [24].

3.3. Reliability and Completeness

The presence of three (possibly four) optical detections amongst the 18 sources which satisfy the IRAC color selection criteria shows that those criteria do not produce a pure brown dwarf sample, and suggests that additional AGN /DOGs may have scattered into the brown dwarf selection region. Monte-Carlo simulations using the existing SDWFS catalog and error distribution were carried out to evaluate the expected level of such contamination.

The pool of 11,907 SDWFS sources was identified which satisfied criterion (iii) in §2.1 and relaxed versions of criteria (i) and (ii), i.e. $[4.5] \leq 19.0$ and $C \equiv [3.6] - [4.5] \geq 1.0$. For each source in this pool, the associated flux errors was used to generate 10,000 realizations of the IRAC photometry and to find the likelihood that each source would meet the full color selection criteria given in §2.1. The summed likelihood of was 67.3, with 34 sources having likelihoods greater than 50% (and a summed likelihood of 26.3). The summed likelihood of selection for the 5202 sources with $1.0 < C < 1.1$ was less than 0.1, indicating contamination from bluer sources is not important. Note that $C > 1$ corresponds to brown dwarf spectral types later than T5 (Patten et al. 2006; Leggett et al. 2010). Visual inspection was carried out in the same manner described in §2.1 for the 86 sources with individual likelihood $\geq 20\%$, and for 40 representative sources with lower likelihoods. Based on this inspection, one third of the sources meeting the color criteria would be classified as artifacts, with the remainder equally divided between objects in or very near the cold brown dwarf color selection space, objects with AGN colors scattering into the selection criteria (e.g., with faint detections at 5.8 and $8.0 \mu\text{m}$), and objects for which the distinction between AGN and cold brown dwarf colors was uncertain. We infer from this that 1/3 to 2/3 of the 18 objects in Table 1 are likely to be objects whose true colors are consistent with cold brown dwarfs, (i.e. that 6 to 12 of the 14 sources in the upper part of Table 1 are likely real brown dwarfs).

A complementary Monte-Carlo calculation was made to assess the completeness of the color-selected sample given typical photometric errors as a function of magnitude for the SDWFS data. The probability that a source would meet the color selection criteria was evaluated using 10,000 realizations of sources as a function of magnitude and color over the range $15 \leq [4.5] \leq 19.5$ and $1.0 \leq [3.6] - [4.5] \leq 2.6$. As expected, the probability is $\sim 50\%$ for bright sources with

$[3.6] - [4.5] = 1.5$. For objects $[3.6] - [4.5] = 1.6$, 90% will be selected at $[4.5] = 17.0$, and 90% of objects with $[3.6] - [4.5] = 1.9$ are selected at $[4.5] = 18.0$. Applying the appropriate percentages as a function of magnitude and color to the sources in the upper part of Table 1, we find an average completeness of $\sim 60\%$.

However it is also the case that warmer brown dwarfs whose true color is bluer than $C = 1.5$ can scatter into the sample. Using models for the true distribution of brown dwarf magnitudes and colors (§3.4) in conjunction with the completeness calculations, we find that this effect closely compensates for losses due to incompleteness. With the finding that sources hotter than T6 do not contribute appreciably, and the reliability estimate, this implies that the true population of cool brown dwarfs meeting the selection criteria is between 6 and 12. Some of these are likely to be unresolved binary brown dwarf systems (see e.g. Burgasser 2007), but this has a relatively small effect on the number density because the increase in numbers due to binaries is compensated for by the larger volume over which they are detectable in a flux limited sample. If a fraction B of the sample is equal mass binaries, the net effect is a reduction of $B(1 - \sqrt{2})/2 \approx 0.3B$ in a volume limited sample. Hence we do not correct for binarity, and in the following section we take 9 brown dwarfs with $C > 1.5$ as representative, of which 8 have $1.5 < C < 2$ and one has $C > 2$.

3.4. Brown Dwarf Counts

We compare our source counts to the models of Burrows et al. (2003), who give a grid of 32 cool brown dwarf models with cooling curves parameterized by mass μ and age t . From the tabulated effective temperature T_{eff} , gravity g and mass we have computed the luminosity L , and set up a linear interpolation in $\log L$ and $\log T_{\text{eff}}$ vs. $\log \mu$ and $\log t$ to give the luminosity and effective temperature for any mass and age.

The expected number N of detectable brown dwarfs can be computed for any mass function and age distribution using the distance r as a function of brown dwarf magnitude m

$$\begin{aligned} r &= 10^{1+(m-M(\mu,t))/5} \\ N &= \Omega \int \int \int p[m, C(\mu, t)] n(\mu, t) r^2 \frac{dr}{dm} dm d\mu dt \end{aligned} \quad (1)$$

where Ω is the survey area, $M(\mu, t)$ is the absolute magnitude as a function of mass and age, $C(\mu, t)$ is the color as a function of mass and age, $n(\mu, t)$ is the number density of brown dwarfs per unit mass and age, and $p(m, C)$ is the probability from the Monte-Carlo completeness calculation in §3.3 of a brown dwarf with magnitude m and color C being selected. In general the number of sources scattered into the acceptance region was quite similar to the number scattered out of the region, so the Monte-Carlo completeness corrections were small.

Assuming a uniform distribution in age between 100 million and 10 billion years, a Chabrier (2003) log normal mass function peaking at $0.079M_{\odot}$, $\Omega = 10 \text{ deg}^2$, and a magnitude limit of $[4.5] < 18.5$ or a flux $> 7.15 \mu\text{Jy}$, the predicted numbers are 55 sources with $1.5 < C < 2$ (where

$C \equiv [3.6] - [4.5]$) and 63 with $C > 2$. Since we estimate only 8 sources are brown dwarfs with $1.5 < C < 2$ and one with $C > 2$, the hypothesis that Chabrier (2003) and Burrows et al. (2003) are both correct can be rejected. There are two problems: the predicted ratio $N(C > 2)/N(1.5 < C < 2) \approx 1.1$ is much higher than the observed 1/8, and the predicted $N(1.5 < C < 2)$ is too high. While power law mass functions ($n \propto M^{-\alpha}$) with α near 0 predict lower counts, the ratio of counts in the color bins is still too high, and has only a weak dependence on α .

However Patten et al. (2006) and Golimoski et al. (2004) show that the observed [4.5] or M -band flux is substantially lower than predicted by these models. This is also apparent in Figure 1. Detailed modeling for the known $C \geq 1.5$ brown dwarfs (e.g. Figure 7 of Leggett et al. 2009) finds $T_{\text{eff}} = 550 - 800\text{K}$ for these objects. The Burrows models for these temperatures predict [3.6] – [4.5] colors which are significantly redder than observed, and [4.5] – [8] colors which are significantly bluer than observed, and suppressing the model [4.5] flux corrects this.

Suppressing the model [4.5] flux has a strong effect on both the ratio problem and the number problem. This flux suppression, presumably due to the CO fundamental at $4.7\mu\text{m}$, has been attributed to non-equilibrium chemistry altering the expected CO absorption depths (Hubeny & Burrows 2007). Suppression of flux in the spectrum causes some backwarming, so the effective temperature increases to

$$T'_{\text{eff}} = T_{\text{eff}} / (1 - S f_2 / R_2)^{1/4} \quad (2)$$

where f_2 is the fraction of the bolometric luminosity in the IRAC channel 2 ([4.5]) detection band from the model, S is the [4.5] suppression, and R_2 is the resolution of the IRAC $4.5\mu\text{m}$ filter. We use $R_2 = 3$ which is somewhat lower than the actual $R_2 = 4.5$, to allow for suppression of flux outside of the [4.5] passband. The $4.5\mu\text{m}$ flux fraction decreases to $f'_2 = (1 - S) f_2 (T'_{\text{eff}})$. Increased suppression decreases the ratio $N(C > 2)/N(1.5 < C < 2)$ and also reduces the expected number counts, as shown by the heavy solid curve in Figure 6. The horizontal band shows the estimated range of 5 to 11 with $1.5 < C < 2$. The lighter solid curve peaking near $S = 0.52$ shows the Poisson likelihood of a given flux suppression based on the numbers seen in the two color bins, assuming that the Chabrier (2003) single object mass function and uniform age distribution are correct. The likelihood is maximized by a suppression of $S = 0.52$. Similar results are obtained for a power law mass function with $\alpha = 1.3$. This suppression of $S = 0.52$ agrees well with the estimate by Golimoski et al. (2004) that the [4.5] flux is suppressed by a factor between 1.5 and 2.5, which corresponds to $S = 0.33$ to 0.60 in our terminology. In other words, suppressing the Burrows et al. (2003) model by a factor of two brings both the models into agreement with both the observed mid-infrared colors and number counts.

Another potential solution is to adopt a different mass function, which, like the predicted luminosities and colors, is not well known for these very low mass objects. Since the Burrows et al. (2003) models give the luminosity vs. mass and age for single brown dwarfs, it is not strictly correct to use system mass functions in these calculations, but to provide a range of examples we have included in Figure 6 both the Chabrier (2003) single object and system mass function, as well as the Bochanski et al. (2009) mass function. Based on SDSS observations of late M dwarfs,

Bochanski et al. (2009) find a log normal mass function peaking at $0.27M_{\odot}$. This results in a much smaller predicted number density of brown dwarfs than for the Chabrier (2003) single object mass function, and requires a smaller $4.5 \mu\text{m}$ flux suppression ($S = 0.26$) to agree with the observed SDWFS counts, as shown by the dotted curves in Figure 6. However, this would not account as well for the observed $4.5\mu\text{m}$ flux discrepancy. The Chabrier (2003) system mass function, which peaks at $0.2M_{\odot}$, shows intermediate results, matching the SDWFS counts for a flux suppression of $S = 0.31$, as shown by the dashed curves in Figure 6. The number density data shown in Bochanski et al. (2009) flatten significantly at the low mass end, so this log normal mass function may not be reliable in the brown dwarf regime. For both the Bochanski et al. (2009) mass function and significant flux suppression of the Burrows models to be correct would suggest that nearly all of the SDWFS brown dwarf candidates are dusty galaxies with no evidence for star formation in the rest UV or mid-IR.

Scaling from the SDWFS counts to the all-sky *WISE* survey, which launched on 2009 Dec. 14, is simpler than comparing to models. The *WISE* sensitivity requirement at $4.6\mu\text{m}$ is $160\mu\text{Jy}$, resulting in a surveyed volume which is $\sim 40\times$ greater than SDWFS, and hence ~ 250 to 500 similarly cool brown dwarfs for a Euclidean distribution. These *WISE* brown dwarfs will be the nearest examples, with correspondingly brighter fluxes and larger parallaxes and proper motions, making followup observations much easier. This should enable a definitive determination of the properties of the ultracool brown dwarf population.

The authors thank Emanuele Daddi, Mark Dickinson, Jason Melbourne, and Tom Soifer for assistance obtaining observations, Nick Seymour for assistance with SDWFS and WIRC reductions, and Vandana Desai for the Mrk 231 spectrum and information about DOG SED's. Tom Soifer, Marcia Rieke, Dan Weedman, and Jim Houck are thanked for allowing access to the GTO MIPS survey of the NDWFS, and we acknowledge Buell Jannuzi's central role in the NDWFS and related surveys of the field. Discussions with Roc Cutri helped us understand the mid-IR characteristics of AGB stars, and Szymon Kozłowski clarified questions about SDWFS variability measurements. We thank the anonymous referee for a detailed and careful review which improved the accuracy of the presentation. This work is based on observations made with the *Spitzer Space Telescope*, which is operated by the Jet Propulsion Laboratory, California Institute of Technology under contract with NASA. This work made use of images and data products provided by the NOAO Deep Wide-Field Survey (NDWFS), which is supported by the National Optical Astronomy Observatory (NOAO), and followup NOAO surveys. NOAO is operated by AURA, Inc., under a cooperative agreement with the National Science Foundation. Some of the data presented herein were obtained at the W.M. Keck Observatory, which is operated as a scientific partnership among Caltech, the University of California and NASA. The Keck Observatory was made possible by the generous financial support of the W.M. Keck Foundation, which also provided support for MB. Some data was obtained at the Hale Telescope, Palomar Observatory as part of a continuing collaboration between Caltech, NASA/JPL, and Cornell University. Support for this work was provided by NASA through an award issued by JPL/Caltech. AHG acknowledges support for this work by the National Science

Foundation (NSF) under Grant No. 0708490. Support for AMG and QK’s contribution to this work was provided by the NSF Science & Technology Center for AO, managed by UCSC (AST-9876783), and the Levine-Leichtman Family Foundation.

Facilities: *Spitzer Space Telescope* (IRAC) (MIPS), Palomar 200” (WIRC), Keck (NIRC2), KPNO (NEWFIRM)

REFERENCES

- Ashby, M. L. N., Stern, D., Brodwin, M., Griffith, R., Eisenhardt, P., et al. 2009, *ApJ*, 701, 428
- Becker, R. H., White, R. L., & Helfand, D. J. 1995, *ApJ*, 450, 559
- Becklin, E. E. & Zuckerman, B. 1988, *Nature*, 336, 656
- Bochanski, J. J., Hawley, S. L., Reid, I. N., Covey, K. R., West, A. A., Golimowski, D. A., & Ivezić, Ž. 2009, in *AIP Conference Series*, ed. E. Stempels, Vol. 1094, 977
- Burgasser, A. J. 2007, *ApJ*, 659, 655
- Burgasser, A. J., Tinney, C. G., Cushing, M. C., Saumon, D., Marley, M. S., Bennett, C. S., & Kirkpatrick, J. D. 2008, *ApJ*, 689, L53
- Burningham, B. et al. 2008, *MNRAS*, 391, 320
- Burrows, A., Sudarsky, D., & Lunine, J. I. 2003, *ApJ*, 596, 587
- Bussmann, R. S. et al. 2009, *ApJ*, 705, 184
- Chabrier, G. 2003, *PASP*, 115, 763
- Cutri, R. M., Low, F. J., Kleinmann, S. G., Olszewski, E. W., Willner, S. P., Campbell, B., & Gillett, F. C. 1989, *AJ*, 97, 866
- Davidge, T. J. & Rigaut, F. 2004, *ApJ*, 607, L25
- de Vries, W. H., Morganti, R., Röttgering, H. J. A., Vermeulen, R., van Breugel, W., Rengelink, R., & Jarvis, M. J. 2002, *AJ*, 123, 1784
- Delorme, P. et al. 2008a, *A&A*, 484, 469
- . 2008b, *A&A*, 482, 961
- Dey, A. et al. 2008, *ApJ*, 677, 943
- Eisenhardt, P. R. et al. 2004, *ApJS*, 154, 48
- Enoch, M. L., Evans, N. J., I.Sargent, A., & Glenn, J. 2009, *ApJ*, 692, 973

- Epchtein, N. et al. 1997, *The Messenger*, 87, 27
- Fazio, G. G. et al. 1998, *SPIE*, 3354, 1024
- . 2004, *ApJS*, 154, 10
- Glass, I. S., Whitelock, P. A., Catchpole, R. M., & Feast, M. W. 1995, *MNRAS*, 273, 383
- Golimoski, D. A. et al. 2004, *ApJ*, 127, 3516
- Hawley, S. L. et al. 2002, *AJ*, 123, 3409
- Hayashi, C. & Nakano, T. 1963, *Prog. Theor. Phys.*, 30, 460
- Houck, J. R. et al. 2005, *ApJ*, 622, L105
- Hubeny, I. & Burrows, A. 2007, *ApJ*, 669, 1458
- Jannuzi, B. T. & Dey, A. 1999, in *Photometric Redshifts and High-Redshift Galaxies*, ed. R. Weymann, L. Storrie-Lombardi, M. Sawicki, & R. Brunner, Vol. 191 (San Francisco: ASP Conference Series), 111
- Kenter, A. et al. 2005, *ApJS*, 161, 9
- Kirkpatrick, J. D. 2005, *ARA&A*, 43, 195
- . 2008, 14th Cambridge Workshop on Cool Stars, Stellar Systems and the Sun, 384, 85
- Kirkpatrick, J. D. et al. 1999, *ApJ*, 519, 834
- Kozlowski, S. et al. 2010, *ApJ*, submitted (astro-ph/1002.3365)
- Kumar, S. S. 1963, *ApJ*, 137, 1121
- Lawrence, A. et al. 2007, *MNRAS*, 379, 1599
- Leggett, S. K. et al. 2009, *ApJ*, 695, 1517
- . 2010, *ApJ*, 710, 1627
- Liu, F. et al. 2008, *SPIE*, 7017, 16
- Lodieu, N., Hambly, N. C., Hambly, R. F., Jameson, R. F., Hodgkin, S. T., Carraro, G., & Kendall, T. R. 2007, *MNRAS*, 374, 372
- Luhman, K. L., Adame, L., D’Alessio, P., Calvet, N., Hartmann, L., Megeath, S. T., & Fazio, G. G. 2005, *ApJ*, 635, L93
- Luhman, K. L. et al. 2006, *ApJ*, 649, 894

- Mauron, N. 2008, *A&A*, 482, 151
- Nakajima, T., Oppenheimer, B. R., Kulkarni, S. R., Golimowski, D. A., Matthews, K., & Durrance, S. T. 1995, *Nature*, 378, 463
- Patten, B. M. et al. 2006, *ApJ*, 651, 502
- Reid, N. 1997, in *ASP Conference Series*, Vol. 127, *Proper Motions and Galactic Astronomy*, ed. R. M. Humphreys, 63
- Rejkuba, M., Minniti, D., Silva, D. R., & Bedding, T. R. 2003, *A&A*, 411, 351
- Robitaille, T. P., Cohen, M., Whitney, B. A., Meade, M., Babler, B., Indebetouw, R., & Churchwell, E. 2007, *AJ*, 134, 2099
- Skrutskie, M. F. et al. 2006, *AJ*, 131, 1400
- Stern, D. et al. 2005, *ApJ*, 631, 163
- . 2007, *ApJ*, 663, 677
- van Dam, M. A. et al. 2006, *PASP*, 118, 310
- Warren, S. J. et al. 2007, *MNRAS*, 381, 1400
- Weights, D. J., Lucas, P. W., Roche, P. F., Pinfield, D. J., & Riddick, F. 2008, *MNRAS*, 392, 817
- Wilson, J. C. et al. 2003, *SPIE*, 4841, 451
- Wizinowich, P. L. et al. 2006, *PASP*, 118, 297
- York, D. G. et al. 2000, *AJ*, 120, 1579
- Zapatero Osorio, M. R., Béjar, V. J. S., Martín, E. L., Rebolo, R., y Navascués, D. B., Mundt, R., Eislöffel, J., & Caballero, J. A. 2002, *ApJ*, 578

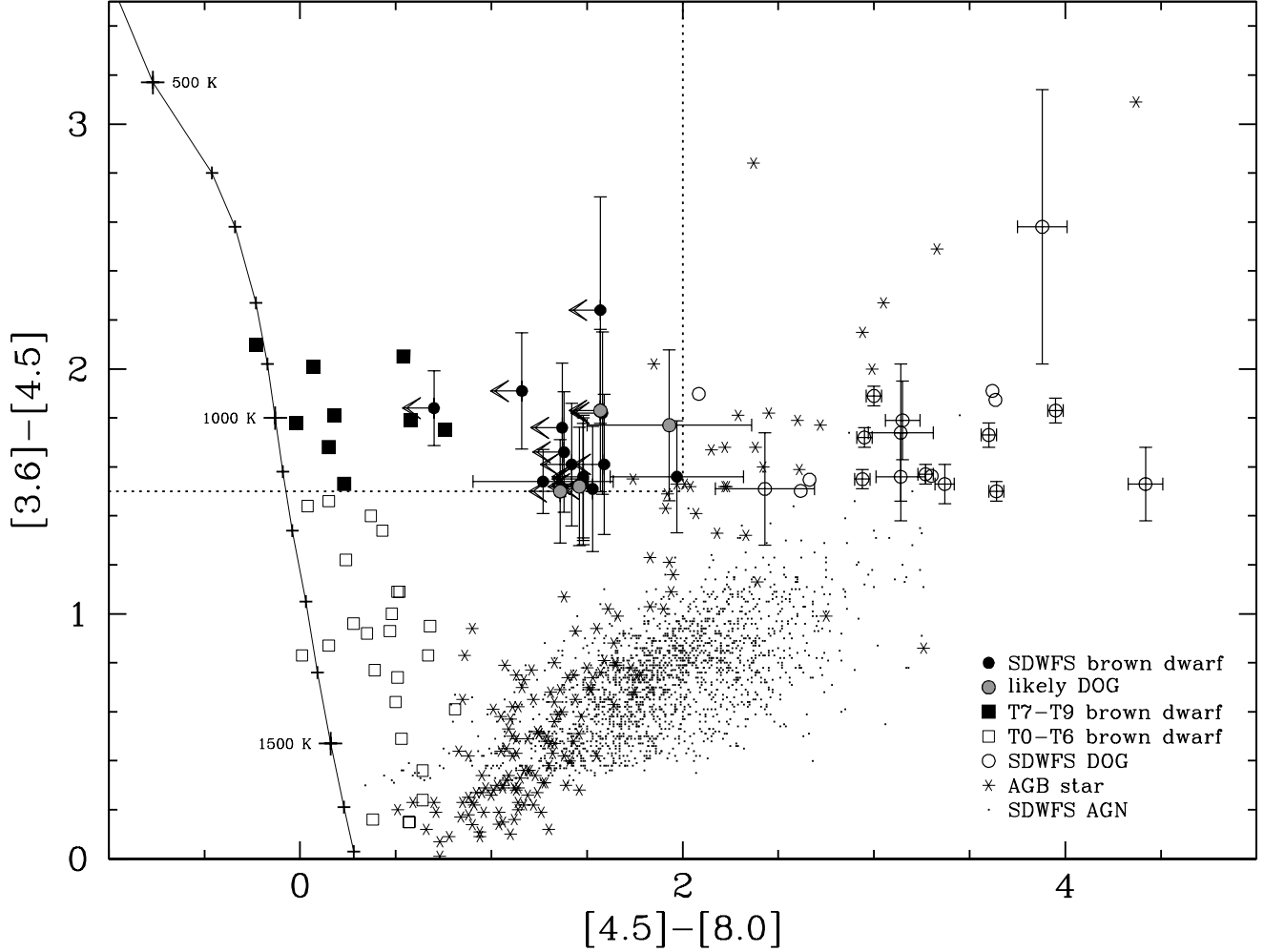


Fig. 1.— IRAC color-color diagram illustrating the selection criteria applied to identify the coolest brown dwarfs (dotted lines). The solid line shows predicted brown dwarf colors models from Burrows et al. (2003) for $T_{\text{eff}} \leq 600\text{K}$ using nonequilibrium, $\log g = 5$ models, and from Hubeny & Burrows (2007) for $T_{\text{eff}} > 600\text{K}$ using nonequilibrium, $\log g = 5$, $\log K_{zz} = 2$, “fast2” CO/CH₄ reaction speed models, with tick marks at 100K intervals from 500 to 1700K. Dots show mid-IR selected AGN selected from the Boötes field using the Stern et al. (2005) IRAC color criteria. Asterisks show variable $8\mu\text{m}$ sources found near the Galactic plane by Robitaille et al. (2007) and thought to be AGB stars. Open squares show spectral class T0 - T6 brown dwarfs from Patten et al. (2006) while filled squares show cooler brown dwarfs from Patten et al. (2006), Warren et al. (2007), Burningham et al. (2008), Burgasser et al. (2008), and Leggett et al. (2010). Black circles show the 14 cool brown dwarf candidates identified in Table 1; arrows show 2σ upper limits based on SDWFS depth at [8]. Open circles show the 14 SDWFS sources with $[3.6] - [4.5] \geq 1.5$ and $[4.5] - [8.0] \geq 2$, which are classified as DOGs. Open circles without error bars are for several DOGs selected by Dey et al. (2008) using $R - [24] > 14$ which did not meet our SDWFS selection criteria (§2.1). Gray circles are objects which meet the cool brown dwarf color criteria but for which optical detections suggest they are DOGs. The brown dwarf candidate near the lower right edge of the selection criteria has a questionable [8] detection, implying it likely has a bluer $[4.5] - [8]$ color than indicated.

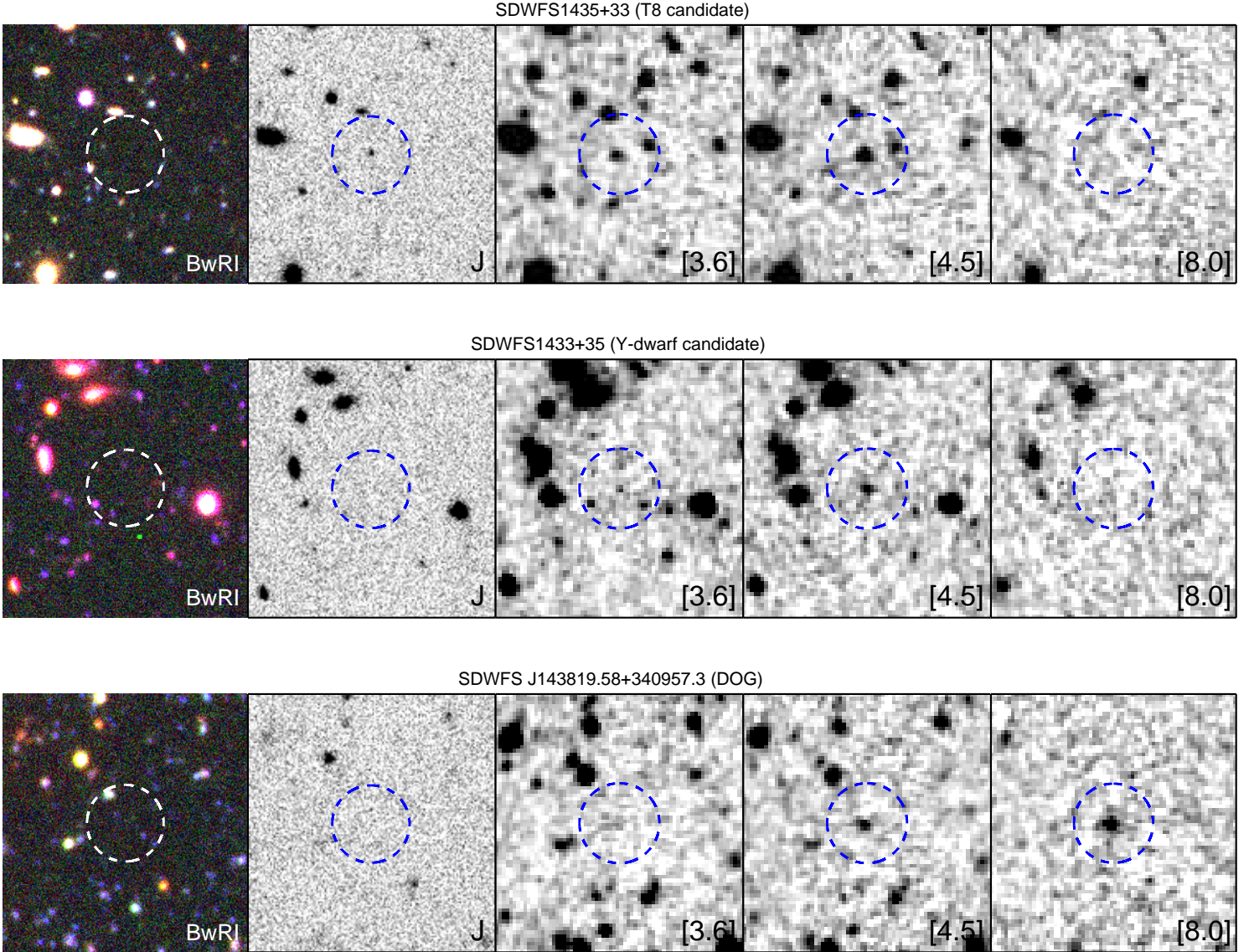


Fig. 2.— Multi-wavelength images of sources with very red $[3.6] - [4.5]$ colors in the SDWFS field. Images are 1 arcmin on a side, with North up and East to the left. The left panels are color composites of the NDWFS B_WRI data, followed by J images from the NEWFIRM survey and IRAC data from SDWFS. Circles are $10''$ in radius, centered on the red IRAC sources. The top strip shows the brightest cool brown dwarf (T8) candidate in SDWFS, while the middle shows the reddest brown dwarf (Y-dwarf) candidate. The bottom strip shows the reddest DOG in SDWFS, which has $[3.6] - [4.5] = 2.58$, but is much redder than the brown dwarf candidates at longer IRAC wavelengths, with $[4.5] - [8.0] = 3.88$.

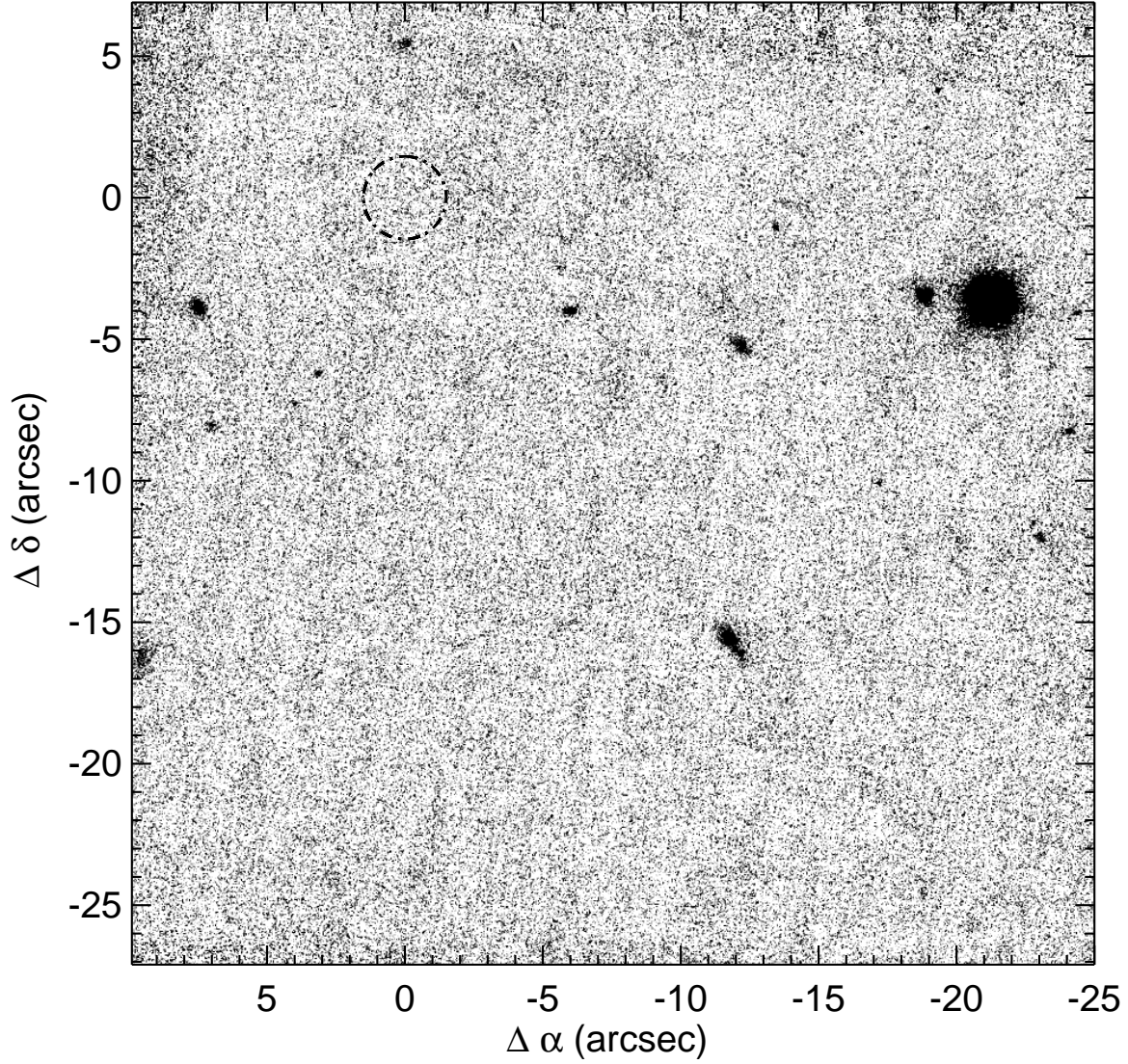


Fig. 3.— H image of the region near SDWFS1433+35 (the Y-dwarf candidate) obtained with the laser guide star adaptive optics system and the NIRC2 camera on the Keck II telescope. The field is $34''$ on a side with North up and East left. The position of the [4.5] source is marked with a $3''$ diameter circle. There are no sources with $\text{SNR} > 2$ within the circle, or with a plausible FWHM.

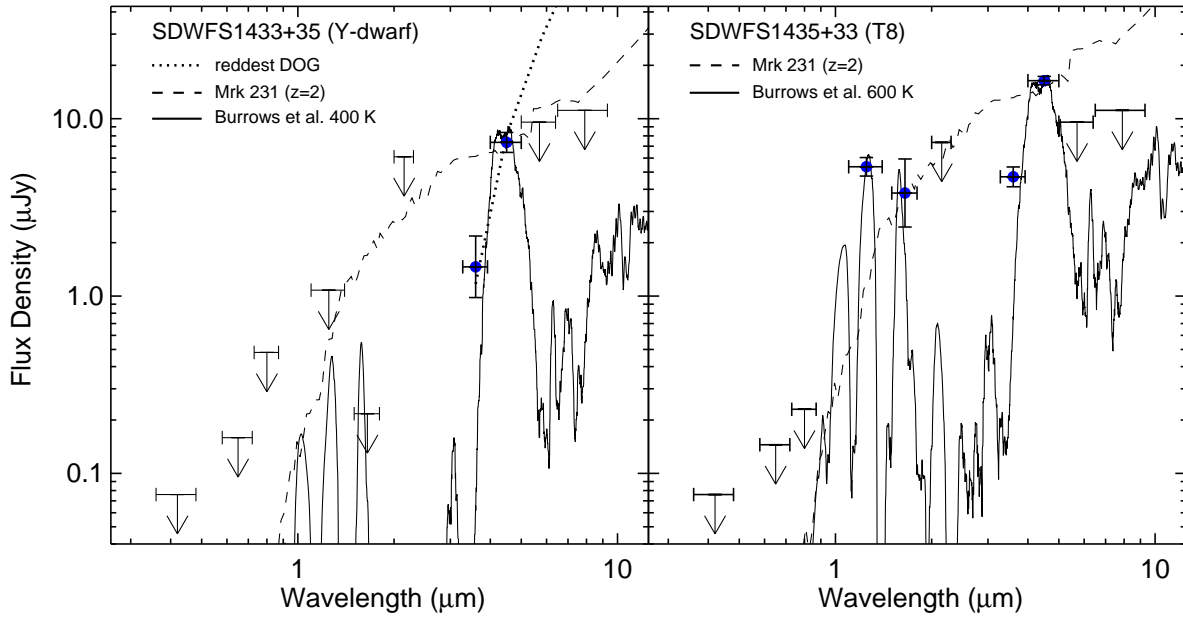


Fig. 4.— SED’s for the Y-dwarf (left) and T8 (right) candidates. The solid line shows 400K (left) and 600K (right) brown dwarf models from Burrows et al. (2003), normalized at $4.5\mu\text{m}$. The models assume non-equilibrium chemistry and $\log(g) = 5.0$. The dashed line shows the spectrum of Mrk 231 at $z = 2$, normalized at $4.5\mu\text{m}$, from Bussmann et al. (2009), representative of DOG SED’s. The dotted line (left) shows the SED for the reddest (in $[3.6] - [4.5]$) DOG found in our search, SDWFS J143819.58+340957.3, which continues to rise steeply beyond $4.5\mu\text{m}$, but is undetected below $3.6\mu\text{m}$.

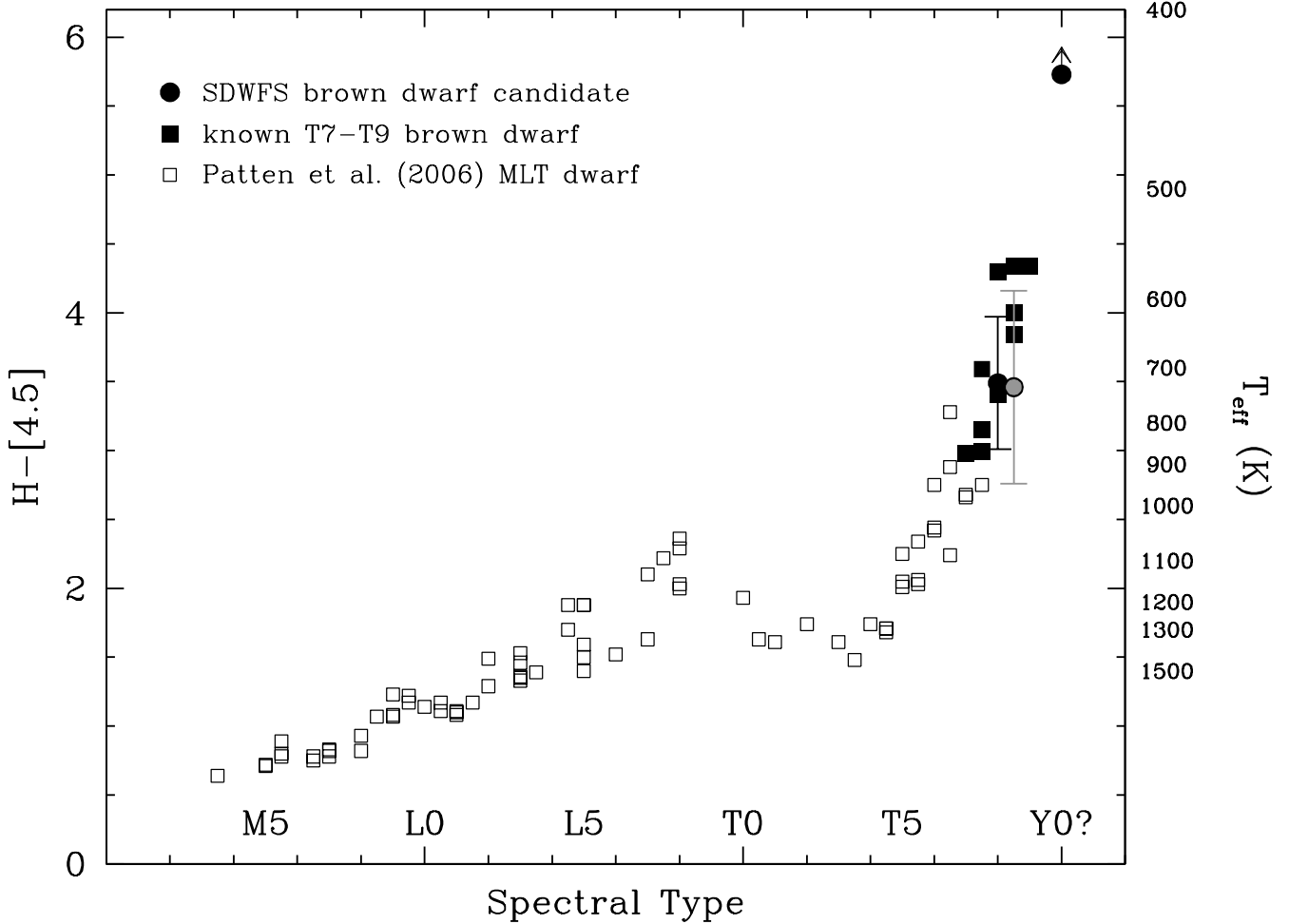


Fig. 5.— $H - [4.5]$ color vs. spectral type for brown dwarfs from Patten et al. (2006) (open squares). Filled squares show data for the published brown dwarfs with $[3.6] - [4.5] \geq 1.5$ from Patten et al. (2006), Warren et al. (2007), Burningham et al. (2008), Burgasser et al. (2008) and Leggett et al. (2010). Filled circles show proposed spectral types and colors for three cool brown dwarfs from this SDWFS study: the observed $H - [4.5]$ for SDWFS J143524.44+335334.6, the lower limit (marked by an arrow) on $H - [4.5]$ for SDWFS J143356.62+351849.2, and the inferred $H - [4.5]$ for SDWFS J143222.82+323746.5 (shown with grey shading) based on its measured J and $[4.5]$ photometry and an assumed $J - H = -0.35$. The error bar for SDWFS1432+32 was increased to match the limit on $H - [4.5]$ given in Table 1. Model temperatures as in Fig. 1 corresponding to $H - [4.5]$ are plotted on the right axis.

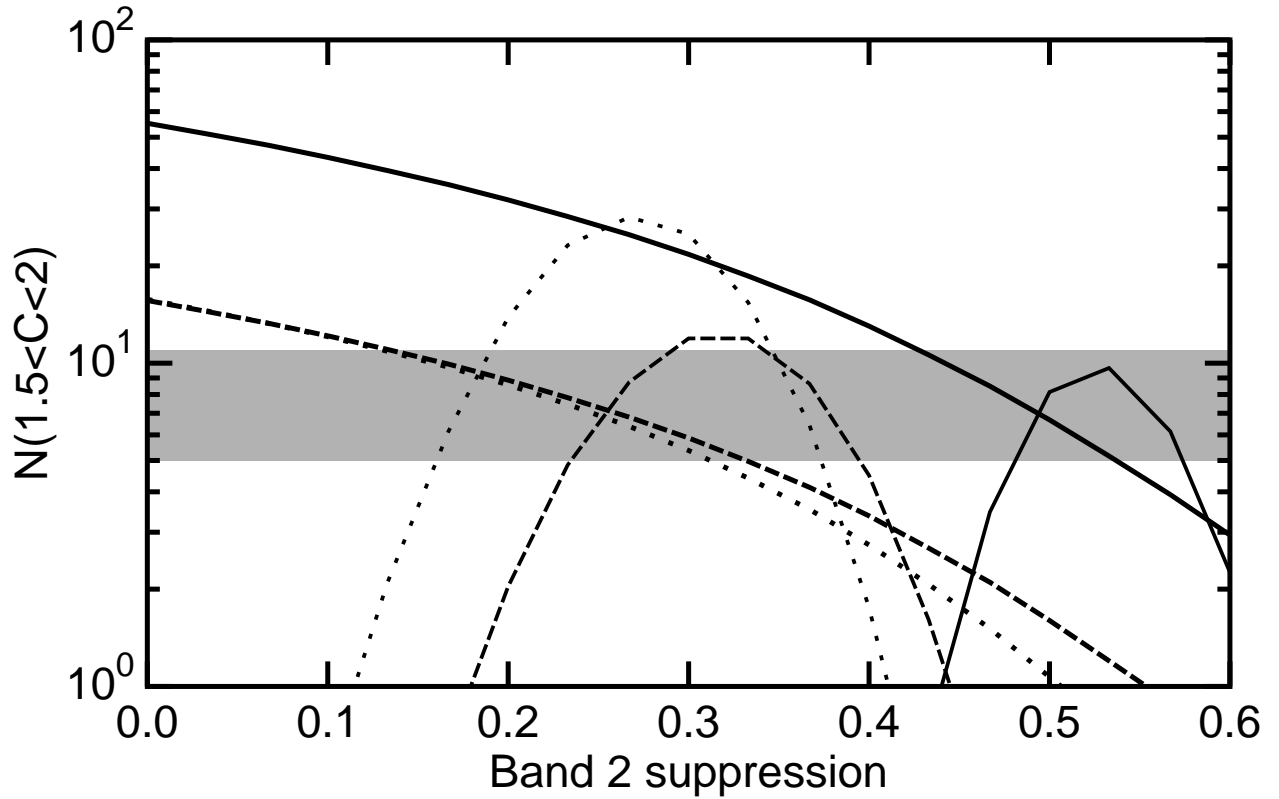


Fig. 6.— The expected number (heavier lines) of SDWFS brown dwarfs in the color range $1.5 < C < 2$, where $C \equiv [3.6] - [4.5]$, and the relative Poisson likelihood (lighter lines) based on the numbers seen with $1.5 < C < 2$ and with $C > 2$, vs. $[4.5]$ flux suppression, for the single object Chabrier (2003, solid), system Chabrier (2003, dashed) and Bochanski et al. (2009, dotted) mass functions. The horizontal band shows the estimated observed number after correcting for contamination.

Table 1. SDWFS Ultracool Brown Dwarf Candidates.

ID	B_W	R	I	J	H	K_s	[3.6]	[4.5]	[5.8]	[8.0]	[3.6] – [4.5]	Notes
SDWFS J142822.12+331056.5	> 25.9	> 24.4	> 22.8	> 22.0	> 20.6	> 19.7	20.03 ± 0.24	18.27 ± 0.11	> 17.7	> 16.9	1.76 ± 0.26	
SDWFS J142831.46+354923.0	> 26.5	> 25.0	> 24.0	> 21.9	> 21.4	> 19.0	19.20 ± 0.11	17.66 ± 0.07	> 17.7	16.39 ± 0.36	1.54 ± 0.13	a
SDWFS J143222.82+323746.5	> 26.7	> 25.6	> 24.5	21.17 ± 0.18	> 20.8	> 20.2	19.97 ± 0.22	18.06 ± 0.09	> 17.7	> 16.9	1.91 ± 0.24	
SDWFS J143355.24+343422.7	> 26.7	> 25.2	> 24.0	> 21.7	> 21.3	> 19.8	20.30 ± 0.30	18.48 ± 0.14	> 17.7	> 16.9	1.82 ± 0.33	b
SDWFS J143356.62+351849.2	> 26.7	> 25.7	> 24.2	> 22.9	> 24.2	> 20.1	20.71 ± 0.44	18.47 ± 0.14	> 17.7	> 16.9	2.24 ± 0.46	c
SDWFS J143524.44+335334.6	> 26.7	> 25.8	> 25.0	21.16 ± 0.13	21.09 ± 0.48	> 19.9	19.44 ± 0.14	17.60 ± 0.06	> 17.7	> 16.9	1.84 ± 0.15	d
SDWFS J143531.65+344509.4	> 26.8	> 24.8	> 24.0	> 21.8	> 20.5	> 20.3	19.94 ± 0.22	18.28 ± 0.11	> 17.7	> 16.9	1.66 ± 0.25	
SDWFS J143555.04+344307.0	> 26.3	> 25.2	> 23.1	> 21.8	> 20.5	> 19.5	19.94 ± 0.22	18.38 ± 0.12	> 17.7	> 16.9	1.56 ± 0.25	
SDWFS J143605.72+342834.5	> 26.6	> 25.3	> 24.6	> 21.9	> 20.9	> 20.0	20.10 ± 0.25	18.49 ± 0.14	> 17.7	> 16.9	1.61 ± 0.29	
SDWFS J143712.48+334516.5	> 25.1	> 23.4	> 21.9	> 21.2	> 21.3	> 20.3	19.93 ± 0.22	18.32 ± 0.12	16.80 ± 0.25	> 16.9	1.61 ± 0.25	e
SDWFS J143724.88+343950.9	> 26.8	> 25.3	> 24.1	> 21.9	> 21.4	> 20.3	19.94 ± 0.22	18.43 ± 0.13	> 17.7	> 16.9	1.51 ± 0.26	f
SDWFS J143749.23+333657.7	> 26.8	> 25.8	> 24.4	> 21.8	> 20.5	> 20.7	19.84 ± 0.20	18.28 ± 0.11	> 17.7	16.31 ± 0.33	1.56 ± 0.23	g
SDWFS J143819.26+334856.5	> 26.4	> 25.3	> 24.5	> 22.1	> 20.6	> 20.2	19.91 ± 0.21	18.38 ± 0.13	17.45 ± 0.45	> 16.9	1.53 ± 0.25	
SDWFS J143821.36+353523.3	> 27.0	> 24.8	> 24.3	> 22.4	> 21.3	> 20.1	19.93 ± 0.22	18.38 ± 0.12	> 17.7	> 16.9	1.55 ± 0.25	h
Likely AGN												
SDWFS J142506.42+350526.0	25.38 ± 0.22	24.43 ± 0.32	> 24.4	> 21.5	> 21.3	> 19.3	20.23 ± 0.28	18.46 ± 0.13	16.96 ± 0.29	16.53 ± 0.41	1.77 ± 0.31	
SDWFS J143334.06+344009.3	25.68 ± 0.31	> 25.3	> 24.3	> 21.7	> 21.5	> 19.8	19.88 ± 0.21	18.36 ± 0.12	17.41 ± 0.44	> 16.9	1.52 ± 0.24	
SDWFS J143359.13+331454.8	25.95 ± 0.41	> 25.8	> 24.6	> 21.8	> 21.6	> 19.8	19.76 ± 0.18	18.26 ± 0.11	> 17.7	> 16.9	1.50 ± 0.21	
SDWFS J143833.76+352209.2	26.55 ± 0.45	> 25.8	> 25.0	> 21.7	> 21.0	> 20.5	20.30 ± 0.30	18.47 ± 0.14	> 17.7	> 16.9	1.83 ± 0.33	

Note. — Photometry is all Vega-based, total magnitudes. Photometry is from NDWFS ($B_W RI$; Jannuzi et al., in prep.), and NEWFIRM (JHK_s ; Gonzalez et al., in prep.). IRAC photometry is from SDWFS (Ashby et al. 2009). Non-detection limits are the 2σ limits for the relevant bands (see §2.1 and 2.2 for details). a: J and H from Palomar (§2.3), K_s from NDWFS; b: marginal J detection; c: Y-dwarf candidate, H from Keck (§2.3); d: T8 candidate; e: Bleed trail makes source questionable; f: [4.5] morphology makes source questionable; g: [8] detection appears spurious; h: Possibly variable.